
Article:
Lu, Jiadong, Hu, Yihua, Liu, Jinglin et al. (1 more author) (2020) Self-Calibration of Phase Current Sensors with Sampling Errors by Multipoint Sampling of Current Values in a Single PWM Cycle. IEEE Transactions on Industrial Electronics. ISSN 0278-0046

https://doi.org/10.1109/TIE.2020.2982110

Self-Calibration of Phase Current Sensors with Sampling Errors by Multipoint Sampling of Current Values in a Single PWM Cycle

Jiadong Lu, *Member, IEEE*, Yihua Hu, *Senior Member, IEEE,* Jinglin Liu, *Member, IEEE,* and Huiqing Wen, Senior *Member, IEEE*

***Abstract*—The accuracy of current sensors is most crucial for the performance of an interior permanent magnet synchronous motor (IPMSM) drive. However, it may have sampling errors that are unavoidable for an actual drive. Therefore, to cope with this problem, this paper proposed a self-calibration strategy for phase-current sensors by utilizing the proposed topology and the correlation among the multiple current values obtained by current sampling values during one single pulse width modulation (PWM) cycle, making minor changes for the cablings of conventional current sensors in the premise of not affecting the normal operation of the drive, and abandoning complex observers or filters for easing computational burden. Besides, its effectiveness was verified by experimental results on a 5kW IPMSM motor prototype, which showed that such sampling errors could be well estimated and eliminated.**

***Index Terms*—Current sampling error, drive, error compensation, interior permanent magnet synchronous motor (IPMSM), inverter, self-calibration.**

I. Introduction

INTERIOR permanent magnet synchronous motor (IPMSM) is attracting more and more attention due to its outstanding features such as high power density, high reliability and high efficiency [1]-[5]. Current measurement is essential for the normal operation of all closed-loop controlled electric machines including induction machines, permanent magnet synchronous machines, and synchronous reluctance machines [6]-[9]. The pre-installed multiple current sensors in IPMSM drives usually include the one at the DC-bus side and the two (at least) at the phase side in a vector-controlled system [10]. The DC-bus current sensor is utilized for over-current protection and the phase current sensors serve as the detecting elements for current closed-loop control [11]. In a sense, the normal operation of these sensors determines the proper operation of the system. If any of them fails, the whole system is likely to collapse [12]-[15]. Under these circumstances, fault-tolerant control (FTC) strategies were proposed and successfully used to solve the problem of current sensor faults [16]-[21].

However, although these sensors are intact, their high measurement accuracy cannot be guaranteed [22], which is a more common reality. The cause behind this phenomenon is the sampling errors of current sensors, which can be explained from two aspects: 1) it is uncertain which sensor is in poor condition (i.e. has a degraded accuracy); 2) it is uncertain how inaccurate the sensor is. The measurement errors of current sensors are usually divided into offset errors and scaling errors [23], which are unavoidable in practice and will degrade system performance [24]. More seriously, these errors and the sampling circuits are probably imbalanced, which may further deteriorate the system performance [25]. All in all, the problem of sampling errors can cause serious consequences. Therefore, many studies have focused on the analysis and compensation of current measurement errors [26]-[35].

In [24] and [26], both band-pass filters (BPFs) and low-pass filters (LPFs) that are used to analyze DC output voltage ripples can be applied to screen out offset and scaling errors. The frequency characteristics of the output voltage in the current closed control loop are utilized to derive the offset and scaling errors in [27]. The speed fluctuation caused by the above mentioned sampling errors will be reflected in the output variable of the speed controller, which is also the reference value for the current controller. Therefore, in [28]-[30], the comparison between the reference and feedback values of the current controller is used to estimate the current measurement errors. In [31], two controllers are established by analyzing the d-q axis currents to estimate the sampling errors of the current sensor. To sum up, all these literatures use the variables within the control loop to estimate the current sensor sampling errors. In [34] and [35], a single current sensor based system is considered for the problem of sampling errors. In these two literatures, offset errors are eliminated by using the current

Manuscript received September 14, 2019; revised February 4, 2020; accepted March 10, 2020. This work was supported by National Natural Science Foundation of China (51907161) and Fundamental Research Funds for the Central Universities (3102019ZDHQD02, 3102019ZDHKY01). *(Corresponding author: Y. Hu).*

J. Lu and J. Liu are with the School of Automation, Northwestern Polytechnical University (NWPU) and Shaanxi Key Laboratory of Small & Special Electrical Machine and Drive Technology of NWPU, Xi'an 710129, China. (E-mail: j.d.lu@nwpu.edu.cn, jinglinl@nwpu.edu.cn).

Y. Hu is with the Department of Electronic Engineering, University of York, York YO10 5DD, U.K. (E-mail: yihua.hu@york.ac.uk).

H. Wen is with the Department of Electrical and Electronic Engineering, Xi'an Jiaotong-Liverpool University, Suzhou 215123, China. (E-mail: Huiqing.Wen@xjtlu.edu.cn).

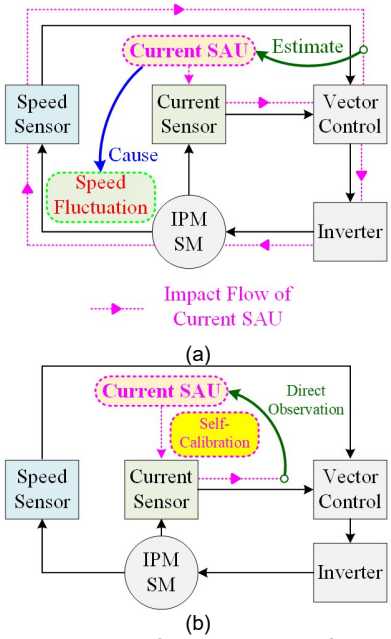

Fig. 1. Common basic ideas of sampling errors of current sensors and calibration method: (a) previous methods, (b) proposed self-calibration method.

characteristics of the single current system on the unique α-β axis.

At present, the main solution of this problem is to analyze its impacts on system performance, such as speed fluctuation or torque ripple. As a torque sensor is not usually installed in the system due to its high cost, the speed feedback information is essential for the aforementioned strategies. This is because the problem of sampling errors causes the speed fluctuation with one and two times the frequency of the fundamental one. The basic ideas of the previous and the newly proposed methods are illustrated in Fig. 1.

In Fig. 1(a), the sampling errors of current sensors can result in the speed fluctuation of the motor, which is in turn utilized to estimate such sampling errors. The involving methods have high requirements for the speed/position sensor. Besides, several observers or digital filters are usually needed to calibrate sampling errors. In this case, three problems will emerge: 1) the computational burden for the main processing unit, which is either a digital signal processor (DSP) or a microprocessor, is increased. 2) It takes a long time to estimate the sampling errors of current sensors, with an estimation accuracy susceptible to load changes. 3) If an inertial load is driven, the schemes for estimation on these sampling errors are likely to fail, because in an inertial system, the problems caused by such sampling errors are mainly reflected in torque ripples rather than in speed fluctuations.

Aiming at solving the aforementioned problems faced by the estimation on sampling errors of current sensors, we proposed in this paper a self-calibration strategy by multipoint sampling of current values in a single PWM cycle, as shown in Fig. 1 (b). The proposed method only requires the current information from one single pulse width modulation (PWM) cycle, with the rest calculation processes conducted only by few operations. This means that it requires neither complex digital filters nor observers. Therefore, the proposed strategy does not add additional computational burden to the system. In addition, its independence from the speed or position feedback information as another feature may prevent its calibration accuracy from being affected by the load type. Besides, it needs no additional hardware devices and does not affect the normal operation of the drive - no matter the PWM generating method or current sampling for control.

The structure of this paper is as follows. In Section II, the problem of the sampling errors of current sensors and the proposed calibration topology are briefly illustrated, respectively. In Sections III & IV, the calibration strategy for both the offset and scaling errors of the two phase-current sensors are analyzed, respectively. In Sections V, the current chopping effect is analyzed. In Section VI, experimental validation is presented. The conclusion is given in Section VII.

II. Proposed Self-Calibration Topology for Sampling Errors of Current Sensors and Its Basic Principles

A. Types of the sampling errors of current sensors

A three-phase three-wire IPMSM drive usually consists of two phase-current sensors, i.e. phase-A & B current sensors. These two sensors can directly measure the corresponding current signals, whereas the phase-C current can only be calculated according to the other two current values ($i_A + i_B + i_C = 0$). This is an ideal situation where there are no sampling errors. By taking the current offset and scaling errors into consideration, the relations between the measured three-phase currents, i_{AM}, i_{BM} and i_{CM}, and the ideal ones, i_A, i_B and i_C, are given by

$$\begin{cases} i_{AM} = k_A \cdot i_A + f_A \\ i_{BM} = k_B \cdot i_B + f_B \\ i_{CM} = -i_{AM} - i_{BM} \end{cases} \quad (1)$$

where k_A, k_B and f_A, f_B are the scaling and offset errors of phase-A & B current sensors, respectively.

It can be seen from (1) that due to the uncertainty of the four parameters for sampling errors of current sensors, the actually measured three-phase current values contain some errors, which will finally degrade the system performance [25]. In an ideal situation, if no such errors exist ($k_A = k_B = 1, f_A = f_B = 0$), the measured three-phase current values will be the same as the ideal ones. Unfortunately, these errors are unavoidable in practice [25]. For this reason, we aim to develop a calibration strategy for these errors in this paper.

B. Proposed Calibration Topology

In this paper, we proposed a self-calibration strategy based on the topology given in Fig. 2. In this figure, i_{DC} as the current at the DC-bus side is used for over-current protection. i_U denotes the current of the DC-bus capacitor. i_P and i_N are the positive and negative currents at the input end of the inverter. Meanwhile, the positive directions of the current sensors are

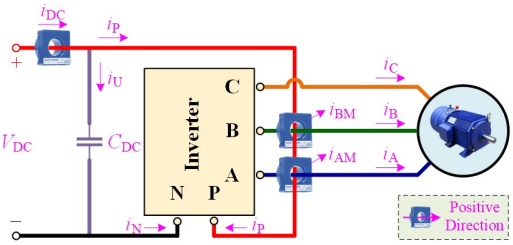

Fig. 2. The proposed self-calibration topology for the sampling errors of phase-current sensors.

also marked in the figure.

Different from the normal installation of the two phase-current sensors, the two phase-current sensors installed in the proposed self-calibration topology not only measure the two phase currents respectively, but also measure i_P at the same time. Besides, by taking the problem of sampling errors into account, the two measured currents i_{AM} and i_{BM} are given as follows:

$$\begin{cases} i_{AM} = k_A \cdot (i_A + i_P) + f_A \\ i_{BM} = k_B \cdot (i_B + i_P) + f_B \end{cases} \quad (2)$$

The relations between i_P and the three-phase currents are given in Table I. In Table I, S_{000}, ..., S_{111} denote the switching states of the inverter, and V_0, ..., V_7 are the corresponding active vectors, respectively.

From Table I, it can be seen that the value of i_P is equal to 0 under the voltage space vector V_0. By substituting this value into (2), we can obtain the value of i_{AM} under the voltage space vector V_0, which is $i_{AM} = k_A \cdot (i_A + i_P) + f_A = k_A \cdot i_A + f_A$. Combining (2) and Table I can obtain the relationship between the measured two currents and the ideal three-phase currents, as shown in Table II, from which it can be seen that the measured two currents are no longer the traditional phase currents, instead, they are related to all the three-phase currents according to the switching states of the inverter. The self-calibration strategy proposed in this paper is based on the relationship given in Table II.

C. Standard Currents Sampling

In Table II, under zero vectors V_0 and V_7, the two current sensors still measure the corresponding normal phase-currents with current sampling errors (please note that these errors exist naturally in actual drives and the ideal phase currents cannot be measured), so the measured two currents are respectively the standard ones. In particular, if there are no current sampling errors, i.e., $k_A = k_B = 1$ & $f_A = f_B = 0$, the measured currents i_{AM} and i_{BM} under zero vectors are equal to the standard currents i_A and i_B, respectively.

Therefore, in this paper, the standard current feedback information is sampled at the middle of each switching period (under the zero vector V_7). It should be noted that although the measured currents i_{AM} and i_{BM} under the zero vector V_7 are not exactly equal to the ideal currents due to sampling errors, they still can be used for current feedback. Whereas if these current sampling errors are too large to be ignored, the system will not be facing the problem of sampling errors of the current sensors. After the calibration of this problem, the measured currents i_{AM} and i_{BM} under the zero vector V_7 will be equal to i_A and i_B, with a small common proportional increment, respectively.

TABLE I
THE RELATIONS BETWEEN THE POSITIVE CURRENT OF THE INVERTER AND THE THREE-PHASE CURRENTS.

Switching States	S_{000} (V_0)	S_{100} (V_1)	S_{110} (V_2)	S_{010} (V_3)	S_{011} (V_4)	S_{001} (V_5)	S_{101} (V_6)	S_{111} (V_7)
i_P	0	i_A	$-i_C$	i_B	$-i_A$	i_C	$-i_B$	0

TABLE II
THE RELATIONSHIP BETWEEN THE MEASURED TWO CURRENTS AND THE IDEAL THREE-PHASE CURRENTS.

Switching States	S_{000} (V_0)	S_{100} (V_1)	S_{110} (V_2)	S_{010} (V_3)
i_{AM}	$k_A \cdot i_A + f_A$	$2k_A \cdot i_A + f_A$	$k_A \cdot (i_A - i_C) + f_A$	$-k_A \cdot i_C + f_A$
i_{BM}	$k_B \cdot i_B + f_B$	$-k_B \cdot i_C + f_B$	$k_B \cdot (i_B - i_C) + f_B$	$2k_B \cdot i_B + f_B$
Switching States	S_{011} (V_4)	S_{001} (V_5)	S_{101} (V_6)	S_{111} (V_7)
i_{AM}	f_A	$-k_A \cdot i_B + f_A$	$k_A \cdot (i_A - i_B) + f_A$	$k_A \cdot i_A + f_A$
i_{BM}	$k_B \cdot (-i_A + i_B) + f_B$	$-k_B \cdot i_A + f_B$	f_B	$k_B \cdot i_B + f_B$

III. OFFSET ERROR CALIBRATION METHOD

In general, the offset and scaling errors regarding to the problem of sampling errors of the current sensors are relatively variables that seldom change within 1 ms in the switching period of the inverter. For a better illustration, in this paper, i_{AM_V0}, ..., i_{AM_V7} and i_{BM_V0}, ..., i_{BM_V7} are the sampled current values of i_{AM} and i_{BM} during the action periods of the basic vectors V_0, ..., V_7, respectively. Moreover, the self-calibration strategy for the offset errors of the two phase-current sensors will be illustrated first in this paper. In addition, the specific methods in the six output voltage sectors (Sector I, ..., VI) are presented as below.

A. Sector I

In Sector I, the conventional seven-segment space vector PWM (SVPWM) technology utilizes the basic vectors V_0, V_1, V_2 and V_7 to generate the output voltage vector. Because the measured currents i_{AM_V0} is equal to i_{AM_V7} according to Table II (the current chopping effect is not considered here), we can obtain three useful current information in Sector I, i.e., i_{AM_V1}, i_{AM_V2} and i_{AM_V7}. The same situation also applies to phase-B current sensor, i.e., i_{BM_V1}, i_{BM_V2} and i_{BM_V7}

$$\begin{cases} i_{AM\_V1} = 2k_A \cdot i_A + f_A \\ i_{AM\_V2} = k_A \cdot (i_A - i_C) + f_A \\ i_{AM\_V7} = k_A \cdot i_A + f_A \end{cases} \quad (3)$$

TABLE III
ESTIMATION EQUATIONS FOR OFFSET ERRORS.

Sector	f_A	f_B
I	$-i_{AM\_V1}+2i_{AM\_V7}$	$i_{BM\_V1}-i_{BM\_V2}+i_{BM\_V7}$
II	$-i_{AM\_V2}+i_{AM\_V3}+i_{AM\_V7}$	$-i_{BM\_V3}+2i_{BM\_V7}$
III	i_{AM_V4}	$-i_{BM\_V3}+2i_{BM\_V7}$
IV	i_{AM_V4}	$-i_{BM\_V4}+i_{BM\_V5}+i_{BM\_V7}$
V	$i_{AM\_V5}-i_{AM\_V6}+i_{AM\_V7}$	i_{BM_V6}
VI	$-i_{AM\_V1}+2i_{AM\_V7}$	i_{BM_V6}

$$\begin{cases} i_{BM\_V1} = -k_B \cdot i_C + f_B \\ i_{BM\_V2} = k_B \cdot (i_B - i_C) + f_B \\ i_{BM\_V7} = k_B \cdot i_B + f_B \end{cases}. \quad (4)$$

It can be seen from (3) and (4) that the offset errors of the two phase-current sensors can be simply extracted from the sampled currents:

$$\begin{cases} f_A = -i_{AM\_V1} + 2i_{AM\_V7} \\ f_B = i_{BM\_V1} - i_{BM\_V2} + i_{BM\_V7} \end{cases}. \quad (5)$$

B. Sectors II, ..., VI

Similar to the situations in Sector I, the two offset errors in Sectors II, ..., VI can also be calculated, which are given in Table III.

IV. CALIBRATION METHOD FOR SCALING ERRORS

In this section, the self-calibration strategy for the scaling errors of the two phase-current sensors is presented, and the specific methods in the six output vector sectors (Sector I, ..., VI) are given.

A. Sector I

The measured currents under the active basic vectors are given in (3) and (4). Here, we define two variables A_{S1} and B_{S1}:

$$\begin{cases} A_{S1} = i_{AM\_V1} - i_{AM\_V2} = -k_A \cdot i_B \\ B_{S1} = i_{BM\_V1} - i_{BM\_V2} = -k_B \cdot i_B \end{cases}. \quad (6)$$

From (6), it can be seen that the relationship between scaling errors k_A and k_B can be easily obtained:

$$\frac{k_A}{k_B} = \frac{A_{S1}}{B_{S1}}. \quad (7)$$

It should be noted that in this paper, the absolute values of k_A and k_B cannot be obtained. Whereas, by applying (7), we can balance the scaling error differences between the two current sensors. Yet what is important is that the detrimental effect of scaling errors on system performances (which cause speed fluctuations and torque ripples with two times the fundamental frequency) can be eliminated upon balancing the scaling errors [27].

TABLE IV
ESTIMATION EQUATIONS FOR SCALING ERRORS.

Sector	k_A/k_B	A_{Sx}	B_{Sx}
I	A_{S1}/B_{S1}	$A_{S1}=i_{AM\_V1}-i_{AM\_V2}$	$B_{S1}=i_{BM\_V1}-i_{BM\_V2}$
II	A_{S2}/B_{S2}	$A_{S2}=i_{AM\_V2}-i_{AM\_V3}$	$B_{S2}=i_{BM\_V2}-i_{BM\_V3}$
III	A_{S3}/B_{S3}	$A_{S3}=i_{AM\_V3}-i_{AM\_V4}$	$B_{S3}=i_{BM\_V3}-i_{BM\_V4}$
IV	A_{S4}/B_{S4}	$A_{S4}=i_{AM\_V4}-i_{AM\_V5}$	$B_{S4}=i_{BM\_V4}-i_{BM\_V5}$
V	A_{S5}/B_{S5}	$A_{S5}=i_{AM\_V5}-i_{AM\_V6}$	$B_{S5}=i_{BM\_V5}-i_{BM\_V6}$
VI	A_{S6}/B_{S6}	$A_{S6}=i_{AM\_V6}-i_{AM\_V1}$	$B_{S6}=i_{BM\_V6}-i_{BM\_V1}$

B. Sectors II, ..., VI

Similar to the situations in Sector I, the relationship between the scaling errors k_A and k_B in Sectors II, ..., VI can also be calculated, which are given in Table IV.

C. Compensation of Scaling Errors

Different from the offset errors, which can be compensated right after the estimation on the current values, the scaling errors have a slightly complicated compensation process. This is because they cannot be directly estimated - only the proportional relationship between the sampling values of all phase-current sensor can be estimated. As a result, more steps need to be carried out to estimate the scaling errors. From Table IV, the value of k_A/k_B is first obtained, and we thus assume that:

$$k = \frac{k_A}{k_B}. \quad (8)$$

The relationship between the two scaling errors is a proportional one. Thus, in order to balance them, we need to multiply and divide their current detection values by the same compensation parameter, respectively. In this paper, we define the compensation parameter as x, and the compensation law is given in (9).

$$\begin{cases} i_A' = x \cdot (k_A \cdot i_A) \\ i_B' = \frac{1}{x} \cdot (k_B \cdot i_B) \end{cases} \quad (9)$$

where i_A' and i_B' are the compensated phase-A & B currents.

The balance law of the proposed method is that the two current sampling values should have the same gain coefficient after balancing. It should be noted that in (9) the offset errors have been compensated in advance. According to the balance law and (9), the value of x can be easily obtained:

$$\begin{aligned} x \cdot k_A &= \frac{1}{x} \cdot k_B \\ \Rightarrow x &= \sqrt{\frac{k_B}{k_A}} \end{aligned}. \quad (10)$$

Finally, the compensation law is given in (11).

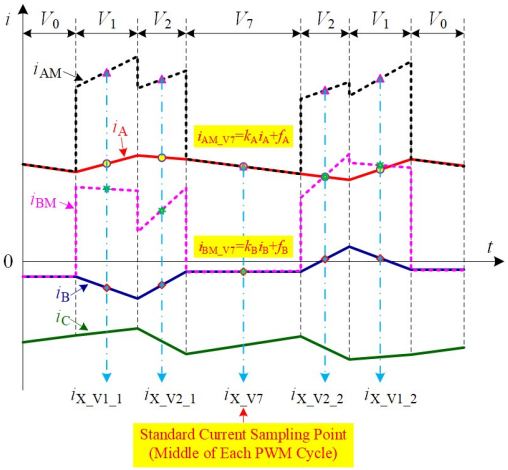

Fig. 3. The current chopping effect on the proposed strategy (Sector I).

$$\begin{cases} i_A' = \sqrt{\dfrac{k_B}{k_A}} \cdot \left(k_A \cdot i_A\right) = \sqrt{k_A \cdot k_B} \cdot i_A \\ i_B' = \sqrt{\dfrac{k_A}{k_B}} \cdot \left(k_B \cdot i_B\right) = \sqrt{k_A \cdot k_B} \cdot i_B \end{cases} \tag{11}$$

V. Current Chopping Effect, Current Measurement Dead Zones and Overall Control Strategy

A. Current Chopping Effect

The information on the proposed calibration strategy for current sampling errors only includes the measured current values within one PWM cycle under different switching states. In this Section, the current chopping effect and the current sampling method will be discussed.

In Section III & IV, we assume that the current chopping effect, which is unavoidable in practice, as shown in Fig. 3, is not considered, i.e., the measured currents are average values. In Fig. 3, which displays the waveforms of the three-phase currents and the two measured ones (Sector I), $i_{X\_V1\_1}$ and $i_{X\_V1\_2}$ are the current sampling values of the X (X stands for A, B, AM, BM) current under the respective two action periods of the vectors V_1 and V_2 (there are two symmetrical periods for V_1 and V_2 in each PWM cycle); i_{X_V7} is the current sampling value of the X current under the action period of the vector V_7.

It can be seen from Fig. 3 that the measured currents are not sampled at the same time, which results in unexpected current sampling errors. The impact of the current chopping effect on the proposed strategy can be explained as follows.

In Table II, Table III and Table IV, the current values of i_{AM_V7} and i_{BM_V7} are all sampled at the middle of each PWM cycle (under the switching state of V_7), which can be regarded as the average values of the corresponding current values during the PWM cycle:

$$\begin{cases} i_{AM\_V7} = k_A \cdot i_{A\_V7} + f_A = k_A \cdot \overline{i_A} + f_A \\ i_{BM\_V7} = k_B \cdot i_{B\_V7} + f_B = k_B \cdot \overline{i_B} + f_B \end{cases}. \tag{12}$$

where $\overline{i_A}$ and $\overline{i_B}$ are the average values of i_A and i_B during the PWM cycle.

However, the values of other currents, i.e., $i_{X\_V1\_1}$, $i_{X\_V1\_2}$, $i_{X\_V2\_1}$ and $i_{X\_V2\_2}$, are not sampled at the middle of the PWM cycle, but at different sampling points in the PWM cycle instead. Therefore, the other current values are not equal to the corresponding average current values in the PWM cycle. Therefore, take i_{AM} as an example, in sector I, $i_{AM\_V1\_1}$ is not equal to i_{AM_V1}. If the current values of $i_{AM\_V1\_1}$ and i_{AM_V7} at different sampling points are used to estimate the offset error of phase A (Sector I), we can obtain the following inequation according to Table II, Table III and the above analysis:

$$\begin{aligned} f_A &= -i_{AM\_V1} + 2i_{AM\_V7} \\ &= -\left(2k_A \cdot \overline{i_A} + f_A\right) + 2i_{AM\_V7} \\ &\neq -\left(2k_A \cdot i_{A\_V1\_1} + f_A\right) + 2i_{AM\_V7} \\ &= -i_{AM\_V1\_1} + 2i_{AM\_V7} \end{aligned} \tag{13}$$

where in this paper $i_{A\_V1\_1}$ and $i_{A\_V1\_2}$ are the transient values of i_A under the two symmetrical action periods of V_1.

From (13), it can be seen that if the transient current values are utilized to replace the average values in the proposed strategy, unexpected errors will emerge in the estimation results. Therefore, in this paper, the average value of the two currents sampled at the symmetrical points on both sides of the PWM midpoint is used to represent the corresponding average current value. Take i_{AM} in sector I as an example, we use the average values of $i_{AM\_V1\_1}$ and $i_{AM\_V1\_2}$ in Fig. 3 to represent the value of i_{AM_V1} (due to the symmetrical current sampling method under the symmetrical PWM):

$$\begin{aligned} i_{AM\_V1} &= 2k_A \cdot \overline{i_A} + f_A \\ &= 2k_A \cdot \left(\frac{i_{A\_V1\_1} + i_{A\_V1\_2}}{2}\right) + f_A \\ &= \frac{2k_A \cdot i_{A\_V1\_1} + f_A}{2} + \frac{2k_A \cdot i_{A\_V1\_2} + f_A}{2} \\ &= \frac{i_{AM\_V1\_1} + i_{AM\_V1\_2}}{2} \end{aligned} \tag{14}$$

In (14), the current processing method is also applicable to the other current sampling values.

B. Current Measurement Dead Zones And Drawbacks of The Proposed Strategy

Due to the dead time of the switching devices, diode recovery time and AD sampling time, the minimum duration T_{min} is required for each switching state, during which an action period for a precise current sampling is needed. Therefore, the regions that can be used to calibrate current sampling errors are limited. From Table III and Table IV, it can be seen that the action time for basic vectors should meet the following requirements: 1) the action time of V_7 (T_7) should be longer than

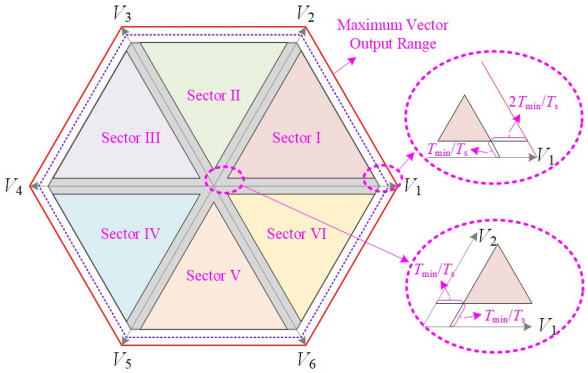

Fig. 4. The output voltage regions (T_s = 100 μs, T_{min} = 5 μs) for current sampling error calibration.

T_{min} during each PWM cycle (T_s), because both i_{AM_V7} and i_{BM_V7} are also used to obtain the standard current feedback values in each PWM cycle, 2) the action time of the two active vectors during the PWM cycle under a calibration command should be both longer than T_{min}. These regions are evenly distributed in the six sectors with colorful shadings (except the one with gray shading) as illustrated in Fig. 4. It should be noted that if the output voltage vector does not fall within the effective region when a calibration command comes, the calibration process for current sampling errors should wait until the output voltage vector falls within the effective region. It should be also pointed out that the normal operation range for the proposed drive (not for calibrating current sampling errors) contains not only the regions with colorful shadings but also those with gray shading (continuous hexagon area). In a word, the calibration strategy can be achieved only when the output voltage vector is located within the six areas with colorful shadings. Also, the output voltage range for normal operation is reduced by $2T_{min}/T_S$ (usually about 10%).

From the above analysis, it can be concluded that although the proposed drive can calibrate current sampling errors with a small amount of calculations, it has two limitations. The first one is that not all output voltage regions can be used to calibrate current sampling errors - each of the six sectors contains an available area that is uniformly distributed. Whereas, the current calibration process that has been delayed by several PWM cycles will have little impact on the system operation. The second one is that in order to obtain standard currents for control, the output voltage range is reduced by $2T_{min}/T_S$, which needs to be heeded in practical application. By setting only one zero voltage vector (either V_0 or V_7) in each PWM cycle, such as the five-segment PWM, the influence of the second defect can be reduced by half (from $2T_{min}/T_S$ to T_{min}/T_S) - see the purple dashed line in Fig. 4 (usually about 95% of the normal output voltage range). To further eliminate the second defect after calibration, the DC-bus cable should be switched by using the relay or an electronic switch to avoid passing through the phase current sensors. And then, the defects during the normal operation can be completely eliminated by making the drive change back to the normal topology.

It should also be noted that the current sensors used in the proposed strategy should be the hall-effect current sensors.

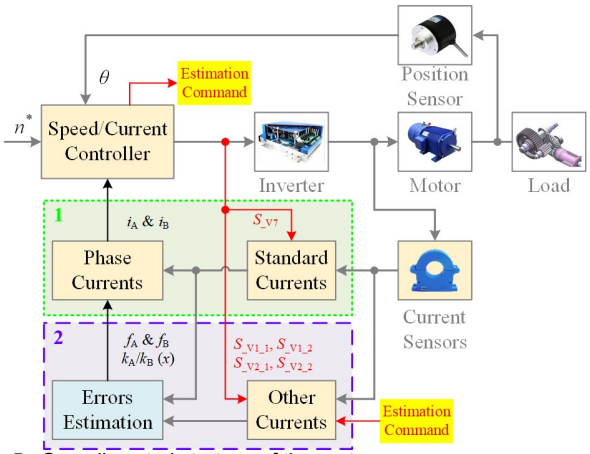

Fig. 5. Overall control strategy of the system.

Whereas the shunt resistors are not applicable.

C. Overall Control Strategy

The overall control strategy is illustrated in Fig. 5. In this figure, S_V7 represents the current sampling point at the middle of each PWM cycle (under the switching period of V_7); S_V1_1, S_V1_2, S_V2_1 and S_V2_2 are the other four current sampling points in Fig. 3 during the PWM cycle for error estimation (take sector I as an example); n^* is the reference speed value; θ is the rotor position, which is used for the double closed-loop control.

In Fig. 5, the controller contains a speed one and a current one, which sends out action commands to the inverter according to the control target and the system feedback variables. The standard currents are sampled at each PWM cycle by using current sampling point S_V7 based on the command sent by the controller (see the green shading dotted square frame marked "1"). Take sector I as an example, according to the control target and operation conditions, the controller sends out a instruction for estimation on current sampling errors, with the other four sampling points, i.e., S_V1_1, S_V1_2, S_V2_1 and S_V2_2. The obtained currents (standard and other currents) are all used to estimate the current sampling errors (see the purple shading dotted square frame marked "2"). Finally, the phase currents i_A and i_B are obtained by using the standard currents and the estimated current sampling errors.

VI. Experimental Validation

In order to validate the effectiveness of the proposed self-calibration strategy for the sampling errors of phase current sensors, an experimental setup is built as displayed in Fig. 6. The main parameters of IPMSM are given in Table V. The system is powered by a three-phase 380 V voltage source with a rectifier and a multi-level output DC-DC converter installed. The measured currents are detected by isolated hall-effect current sensors (HS01-100). The analog-to-digital converter (AD) within the controller TMS320F28335 is a 12-bit one with the conversion time of about 1 μs. The inverter is an integrated power module (Mitsubishi PM75RLA120). The load is controlled by a dynamometer. All the current values are re-detected by the current clamps for comparison. The sampling errors of current sensors are artificially introduced to

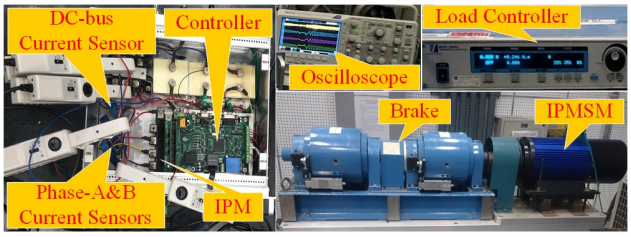

Fig. 6. The experimental setup.

TABLE V
MAIN PARAMETERS OF IPMSM FOR EXPERIMENT.

Parameter	Value	Parameter	Value
Rated power	5 kW	Pole pairs	3
Inverter DC voltage	540 V	*d*-axis Inductance	4.2 mH
Rated voltage	380 V	*q*-axis Inductance	10.1 mH
Rated current	8.5 A	Phase resistance	0.18 Ω
Efficiency	0.9	Maximum speed	3000 r/min
Rated torque	15 N·m	Voltage constant	125 V/(kr/min)

TABLE VI
THE PARAMETERS OF SAMPLING ERRORS OF CURRENT SENSORS.

Parameter	Value	Parameter	Value
f_A	1.5 A	f_B	-2 A
k_A	0.9	k_B	1.2

the system, and their parameters are given in Table VI.

The phase-A & B currents in steady state with the problem of sampling errors are displayed in Fig. 7. When the motor runs at 3000 r/min with 15 N·m load, it can be seen that the actual phase currents fluctuate obviously with unbalanced waveforms.

The actual d-q axis currents with the problem of sampling errors are displayed in Fig. 8. The ripples on the d-q axis currents caused by this problem decrease the system performance.

The motor output speed (n) and its harmonic components with the problem of sampling errors are displayed in Fig. 9. It can be seen from Fig. 9 (a) that the speed ripple caused by this problem reaches ±40 r/min. By fast fourier transform (FFT), the harmonic components of the output speed are given in Fig. 9 (b). As can be noticed, the main harmonic orders are one and two times the fundamental frequency components, which reach 6 r/min and 11 r/min respectively. This is the same as what has been pointed out in the Introduction Section.

The waveforms of i_{AM} and i_{BM} with the problem of sampling errors are displayed in Fig. 10. During this period, the output voltage vector is within Sector VI, the PWM cycle period (T_s) is marked with yellow shadow, and the action vectors of the seven-segment SVPWM are V_0, V_1, V_6, V_7, V_6, V_1 and V_0, respectively. According to the proposed strategy in Sector VI, i_{XM_V1} and i_{XM_V6} are sampled for calibration. i_{XM_V7} is utilized for both the closed-loop control and calibration.

The measured current values are given in Table VII. The estimated parameters of the sampling errors of all current

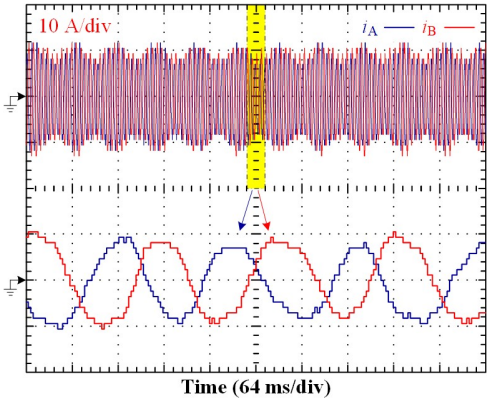

Fig. 7. Actual phase-A & B currents in steady state (n=3000 r/min) with the problem of sampling errors.

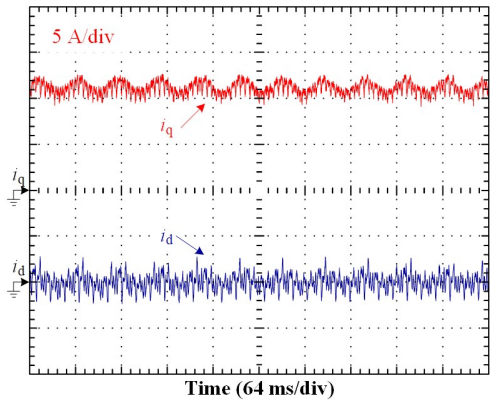

Fig. 8. Actual d-q axis currents with the problem of sampling errors.

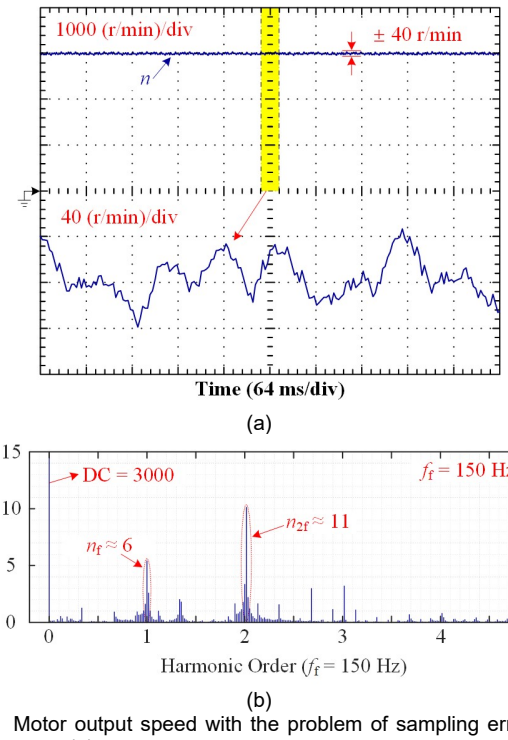

Fig. 9. Motor output speed with the problem of sampling errors: (a) output speed, (b) harmonic components.

sensors are also given in Table VII. Compared with the artificially introduced parameters, the estimated ones have high

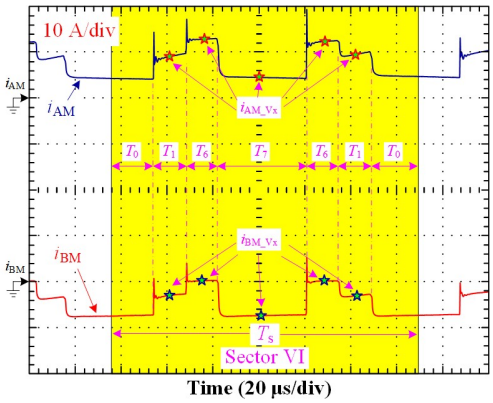

Fig. 10. Actually detected waveforms of i_{AM} and i_{BM} with the problem of sampling errors (Sector VI).

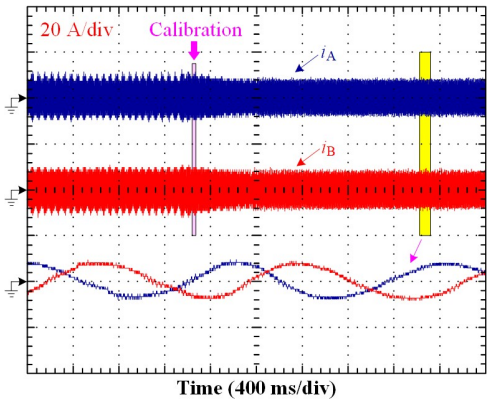

Fig. 11. The phase-A & B currents during the calibration.

TABLE VII
THE MEASURED CURRENT VALUES AND THE ESTIMATED SAMPLING ERRORS OF CURRENT SENSORS.

Parameter	Value	Parameter	Value
i_{AM_V1}	9.93 A	i_{BM_V1}	-6.19 A
i_{AM_V6}	12.96 A	i_{BM_V6}	-2.05 A
i_{AM_V7}	5.70 A	i_{BM_V7}	-11.49 A
f_A'	1.47 A	f_B'	-2.05 A
$f_A' - f_A$	-0.03 A	$f_B' - f_B$	0.06 A
k_A'/k_B'	0.73	$(k_A'/k_B')/(k_A/k_B)$	0.98

estimation precision.

It should be noted that the estimation accuracy of the problem of sampling errors depends on several factors - first, the artificially introduced parameters of sampling errors for current sensors are not exactly the same as the actual ones; second, random sampling errors; third, other kinds of problems of sampling errors that are not considered in this paper.

By applying the proposed calibration strategy to the sampling errors, the waveforms of phase-A & B currents with the problem of sampling errors are presented in Fig. 11. It can be seen from this figure that after calibration, the phase-currents become balanced again. Therefore, the detrimental effect of this problem on the system performance can be finally eliminated.

The information on the motor output speed and its FFT analysis is given in Fig. 12. It can be seen from Fig. 12 (a) that the speed ripples are reduced from ±40 r/min to ±5 r/min. The remaining speed ripples may be caused by the imperfect control effect of the system. The FFT analysis of the output speed is given in Fig. 12 (b). It can be seen that the main harmonic components in Fig. 9 (b) are eliminated. Particularly, the first and second-order harmonic components are reduced from 6 r/min and 11 r/min to smaller than 0.01 r/min, with the maximum harmonic component of about 0.05 r/min. This means that good system performance is guaranteed.

By testing the estimation results under small sampling errors, which are given in Table VIII, the currents and speed show minor differences compared with the normal ones. However, the FFT analysis of torque ripples in Fig. 13 (a) shows that the main effect is reflected in the torque ripples under this

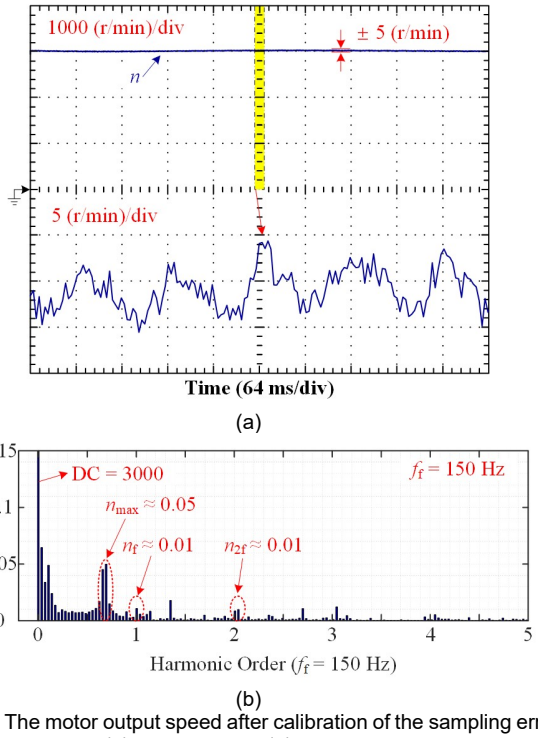

Fig. 12. The motor output speed after calibration of the sampling errors of current sensors: (a) output speed, (b) harmonic component.

TABLE VIII
THE PARAMETERS OF SMALL SAMPLING ERRORS.

Parameter	Value	Parameter	Value
f_A	0.15 A	f_B	-0.2 A
k_A	0.95	k_B	1.05

condition, and that the one (T_f) and two times (T_{2f}) the fundamental frequency components are significant.

By applying the proposed strategy, the estimated current sampling errors are displayed in Table IX. It can be seen from this table that the estimated results are not good as the results in Table VII, but they can still reduce the current sampling errors to a certain degree. The FFT analysis of the torque ripples is illustrated in Fig. 13 (b). It can be seen from this figure that the components with one and two times of the fundamental frequency are almost eliminated.

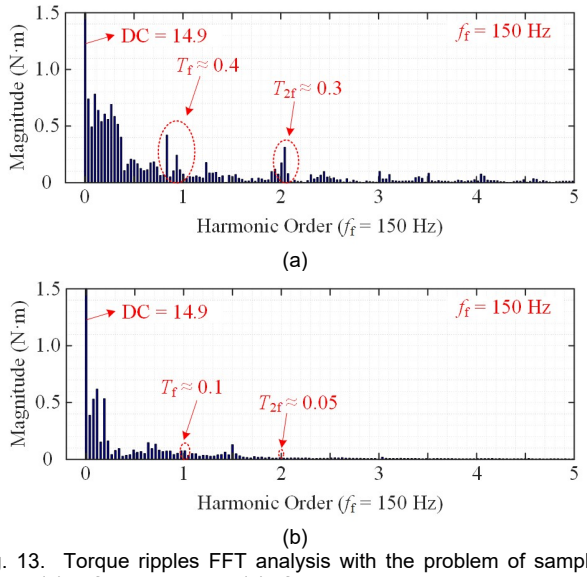

Fig. 13. Torque ripples FFT analysis with the problem of sampling errors: (a) before calibration, (b) after calibration.

VII. Conclusion

In order to solve the problem of sampling errors of the current sensors that degrades system performance, this paper proposes a self-calibration strategy for phase-current sensors. The proposed strategy applies a topology that has been slightly changed based on the traditional one, in the premise of not affecting the normal operation of the system. Its effectiveness is verified by experimental results on a 5-kW IPMSM prototype. Phase-current waveforms are greatly improved after calibration of the problem above mentioned. The experimental results demonstrate that the speed ripples are significantly reduced by 87.5%.

1) The proposed calibration strategy to tackle the above-mentioned problem can be realized within 1 ms in one single PWM cycle.
2) The proposed strategy can be simply extended to other situations where all phase-current sensors are installed.
3) The normal operation of the system is not affected by applying the proposed strategy.
4) The proposed strategy accomplishes the online calibration of the problem of sampling errors of current sensors, while abandoning complicated observers and filters, which results in a simpler algorithm.
5) The proposed strategy might be applied to other types of motor drives by modification.
6) Good electromagnetic isolation measures can prevent the inverter itself and the additional cables from electromagnetic interference to the system.

TABLE IX
The Estimated Values of Small Sampling Errors.

Parameter	Value	Parameter	Value
f_A'	0.09 A	f_B'	-0.28 A
$f_A' - f_A$	-0.06 A	$f_B' - f_B$	-0.08 A
k_A'/k_B'	0.93	$(k_A'/k_B')/(k_A/k_B)$	1.03

References

[1] G. L. Wang, J. Y. Kuang, N. N. Zhao, G. Q. Zhang, and D. G. Xu, "Rotor position estimation of PMSM in low speed region and standstill using zero voltage vector injection," *IEEE Trans. Power Electron.,* vol. 33, no. 9, pp. 7948 - 7958, Sep. 2018.

[2] C. Gong, Y. H. Hu, K. Ni, J. L. Liu, and J. Q. Gao, "SM load torque observer based FCS-MPDSC with single prediction horizon for high dynamics of surface-mounted PMSM," *IEEE Trans. Power Electron.*, vol. 35, no. 1, pp. 20-24, Jan. 2020.

[3] C. L. Xia, Z. Q. Li, and T. N. Shi, "A Control Strategy for Four-Switch Three-Phase Brushless DC Motor Using Single Current Sensor," *IEEE Trans. Ind. Electron.,* vol. 56, no. 6, pp. 2058-2066, June 2009.

[4] G. L. Wang, D. X. Xiao, G. Q. Zhang, C. R. Li, X. G. Zhang, and D. G. Xu, "Sensorless control scheme of IPMSMs using HF orthogonal square-wave voltage injection into a stationary reference frame," *IEEE Trans. Power Electron.,* vol. 34, no. 3, pp. 2573-2584, Mar. 2019.

[5] C. Gong, Y. H. Hu, G. P. Chen, H. Q. Wen, Z. Wang, and K. Ni, "A DC-bus capacitor discharge strategy for PMSM drive system with large inertia and small system safe current in EVs," *IEEE Trans. Ind. Informat.*, vol. 15, no. 8, pp. 4709 - 4718, Aug. 2019.

[6] L. Jarzebowicz, "Errors of a linear current approximation in high-speed PMSM drives," *IEEE Trans. Power Electron.,* vol. 32, no. 11, pp. 8254-8257, Nov. 2017.

[7] C. L. Xia, D. Wu, T. N. Shi, and W. Chen, "A current control scheme of brushless DC motors driven by four-switch three-phase inverters," *IEEE J. Em. Sel. Top. P.,* vol. 5, no. 1, pp. 547-558, Mar., 2017.

[8] S. N. Vukosavic, L. S. Peric, and E. Levi, "Digital current controller with error-free feedback acquisition and active resistance," *IEEE Trans. Ind. Electron.,* vol. 65, no. 3, pp. 1980-1990, Mar., 2018.

[9] X. Li, S. Dusmez, B. Akin, and K. Rajashekara, "A new SVPWM for the phase current reconstruction of three-phase three-level T-type converters," *IEEE Trans. Power Electron.,* vol. 31, no. 3, pp. 2627-2637, Mar. 2016.

[10] Y. X. Xu, H. Yan, J. B. Zou, B. C. Wang, and Y. H. Li, "Zero voltage vector sampling method for PMSM three-phase current reconstruction using single current sensor," *IEEE Trans. Power Electron.,* vol. 32, no. 5, pp. 3797-3807, May 2017.

[11] Q. P. Tang, A. W. Shen, W. H. Li, P. Luo, M. Chen, and X. N. He, "Multiple-positions-coupled sampling method for PMSM three-phase current reconstruction with a single current sensor," *IEEE Trans. Power Electron.,* vol. 35, no. 1, pp. 699-708, Jan. 2020.

[12] C. Y. Wu, C. Q. Guo, Z. W. Xie, F. L. Ni, and H. Liu, "A signal-based fault detection and tolerance control method of current sensor for PMSM drive," *IEEE Trans. Ind. Electron.,* vol. 65, no. 12, pp. 9646-9657, Dec., 2018.

[13] Y. Yu, Y. Z. Zhao, B. Wang, X. L. Huang, and D. G. Xu, "Current sensor fault diagnosis and tolerant control for VSI-based induction motor drives," *IEEE Trans. Power Electron.*, vol. 33, no. 5, pp. 4238 - 4248, May 2018.

[14] C. M. Wolf, M. W. Degner, and F. Briz, "Analysis of current sampling errors in PWM VSI drives," *IEEE Trans. Ind. Appl.*, vol. 51, no. 2, pp. 1551 - 1560, Mar./Apr. 2015.

[15] W. Wang, Y. Feng, Y. Shi, M. Cheng, W. Hua, and Z. Wang, "Fault-tolerant control of primary permanent-magnet linear motors with single phase current sensor for subway applications," *IEEE Trans. Power Electron.*, vol. 34, no. 11, pp. 10546 - 10556, Nov. 2019.

[16] M. Manohar and S. Das, "Current sensor fault-tolerant control for direct torque control of induction motor drive using flux-linkage observer," *IEEE Trans. Ind. Informat.,* vol. 13, no. 6, pp. 2824-2833, Dec., 2017.

[17] C. Chakraborty and V. Verma, "Speed and current sensor fault detection and isolation technique for induction motor drive using axes transformation," *IEEE Trans. Ind. Electron.,* vol. 62, no. 3, pp. 1943-1954, Mar., 2015.

[18] F. R. Salmasi, "A self-healing induction motor drive with model free sensor tampering and sensor fault detection, isolation, and compensation," *IEEE Trans. Ind. Electron.*, vol. 64, no. 8, pp. 6105 - 6115, Aug. 2017.

[19] X. Q. Wang, Z. Wang, Z. X. Xu, M. Cheng, W. Wang, and Y. H. Hu, "Comprehensive diagnosis and tolerance strategies for electrical faults

and sensor faults in dual three-phase PMSM drives," *IEEE Trans. Power Electron.,* vol. 34, no. 7, pp. 6669-6684, Jul. 2019.
[20] K. Him and T. M. Jahns, "Phase current reconstruction for AC motor drives using a DC link single current sensor and measurement voltage vectors," *IEEE Trans. Power Electron.,* vol. 21, no. 5, pp. 1413-1419, Sep. 2006.
[21] J. I. Ha, "Current prediction in vector-controlled PWM inverters using single DC-link current sensor," *IEEE Trans. Ind. Electron.,* vol. 57, no. 2, pp. 716-726, Feb. 2010.
[22] C. H. Choi, K. R. Cho, and J. K. Seok, "Inverter nonlinearity compensation in the presence of current measurement errors and switching device parameter uncertainties," *IEEE Trans. Power Electron.,* vol. 22, no. 2, pp. 576-583, Mar. 2007.
[23] N. B. Belayneh, C. H. Park, and J. M. Kim, "Compensation of arm current sensor errors in modular multilevel converter," *IEEE Trans. Ind. Appl.*, vol. 55, no. 5, pp. 5005 - 5012, Sep./Oct. 2019.
[24] Q. N. Trinh, P. Wang, Y. Tang, L. H. Koh, and F. H. Choo, "Compensation of DC offset and scaling errors in voltage and current measurements of three-phase AC/DC converters," *IEEE Trans. Power Electron.,* vol. 33, no. 6, pp. 5401-5414, Jun. 2018.
[25] S. X. Xiao, T. N. Shi, X. M. Li, Z. Q. Wang, and C. L. Xia, "Single-current-sensor control for PMSM driven by quasi-Z-source inverter," *IEEE Trans. Power Electron.,* vol. 34, no. 7, pp. 7013-7024, Jul. 2019.
[26] Q. N. Trinh, F. H. Choo, Y. Tang, and P. Wang, "Control strategy to compensate for current and voltage measurement errors in three-phase PWM rectifiers," *IEEE Trans. Ind. Appl.*, vol. 55, no. 3, pp. 2879 - 2889, May/Jun. 2019.
[27] M. Kim, S. K. Sul, and J. Lee, "Compensation of current measurement error for current-controlled PMSM drives," *IEEE Trans. Ind. Appl.*, vol. 50, no. 5, pp. 3365 - 3373, Sep./Oct. 2014.
[28] D. W. Chung and S. K. Sul, "Analysis and compensation of current measurement error in vector-controlled AC motor drives," *IEEE Trans. Ind. Appl.*, vol. 34, no. 2, pp. 340 - 345, Mar./Apr. 1998.
[29] K. W. Lee and S. I. Kim, "Dynamic performance improvement of a current offset error compensator in current vector-controlled SPMSM drives," *IEEE Trans. Ind. Electron.,* vol. 66, no. 9, pp. 6727-6736, Sep., 2019.
[30] H. S. Jung, S. H. Hwang, J. M. Kim, C. U. Kim, and C. Choi, "Diminution of current-measurement error for vector-controlled ac motor drives," *IEEE Trans. Ind. Appl.*, vol. 42, no. 5, pp. 1249 - 1256, Sep./Oct. 2006.
[31] Q. N. Trinh, P. Wang, Y. Tang, and F. H. Choo, "Mitigation of DC and harmonic currents generated by voltage measurement errors and grid voltage distortions in transformerless grid-connected inverters," *IEEE Trans. Energy Convers.,* vol. 33, no. 2, pp. 801-813, Jun. 2018.
[32] S. N. Vukosavić, L. S. Perić, and E. Levi, "AC current controller with error-free feedback acquisition system," *IEEE Trans. Energy Convers.,* vol. 31, no. 1, pp. 381-391, Mar. 2016.
[33] M. C. Harke and R. D. Lorenz, "The spatial effect and compensation of current sensor differential gains for three-phase three-wire systems," *IEEE Trans. Ind. Appl.*, vol. 44, no. 4, pp. 1181 - 1189, Jul./Aug. 2008.
[34] Y. Cho, T. LaBella, and J. S. Lai, "A three-phase current reconstruction strategy with online current offset compensation using a single current sensor," *IEEE Trans. Ind. Electron.,* vol. 59, no. 7, pp. 2924-2933, Jul. 2012.
[35] H. Yan, Y. X. Xu, W. D. Zhao, H. Zhang, and C. Gerada, "DC drift error mitigation method for three-phase current reconstruction with single hall current sensor," *IEEE Trans. Magn.,* vol. 55, no. 2, pp. 8100604, Feb. 2019.

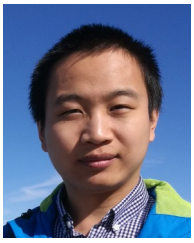

Jiadong Lu (M'19) was born in Pucheng, China, 1990. He received the B.S., the M.S. and the Ph.D. degrees in electrical engineering from Northwestern Polytechnical University (NWPU), Xi'an, China in 2012, 2015 and 2018, respectively. Between 2017 and 2018, he was with the Department of Electrical Engineering, Electronics and Computer Science, University of Liverpool (UoL), U.K. as an Honorary Academic Researcher. Currently, he is an Associate Research Fellow at the Department of Electrical Engineering, NWPU.

His research interests include hybrid-fault-tolerant control techniques for permanent magnet synchronous motor drives, aging issue for motor drives and power electronics converters & control.

Yihua Hu (M'13-SM'15) received the B.S. degree in electrical engineering in 2003, and the Ph.D. degree in power electronics and drives in 2011, both at China University of Mining and Technology. Between 2011 and 2013, he was with the College of Electrical Engineering, Zhejiang University as a Postdoctoral Fellow. Between 2013 and 2015, he worked as a Research Associate at the power electronics and motor drive group, the University of Strathclyde. Between 2016 and 2019, he was a Lecturer at the Department of Electrical Engineering and Electronics, University of Liverpool (UoL). Currently, he is a reader at Electronics Engineering Department at University of York (UoY). He has published 85 papers in IEEE Transactions journals. His research interests include renewable generation, power electronics converters & control, electric vehicle, more electric ship/aircraft, smart energy system and non-destructive test technology. He is the associate editor of IEEE Transactions on Industrial Electronics, IET Renewable Power Generation, IET Intelligent Transport Systems and Power Electronics and Drives.

Jinglin Liu (M'01) received the B.Eng. degree in electrical engineering from Tsinghua University, Beijing, China, in 1986, and the M.Eng. and the Ph.D. degrees in electrical engineering from NWPU, Xi'an, China, in 1990 and 2002, respectively. Since 1994, he has been a Faculty Member with NWPU, Xi'an, where he is currently a Professor of Electrical Engineering. His research interests include electrical machines design and drives, power electronics, fault diagnosis, and motion control.

Huiqing Wen (M'13-SM'18) received his B.S. and M.S. degrees in Electrical Engineering from Zhejiang University, Hangzhou, China, in 2002 and 2006; and his Ph.D. degree in Electrical Engineering from the Chinese Academy of Sciences, Beijing, China, in 2009. From 2009 to 2010, he was an Electrical Engineer working in the Research and Development Center, GE (China) Co., Ltd., Shanghai, China. He is presently working as an Associate Professor at the Xi'an Jiaotong-Liverpool University, Suzhou, China. His current research interests include power electronics and renewable energy.